Thermal Properties of Polyurethane (PU) Through Molecular Dynamics (MD) Simulations

Industry Mentors (Dow Chemical Company): Dr. Tom Fielitz, Dr. Puja Agarwala

Course TA: Jay Shah

CHEG/CISC/ECEG/MSEG 848

Spring 2025

Prof. Arthi Jayaraman

May 15, 2025

Tristan Myers	Tamem Salah	Siyuan Liu
Ph.D. student	Ph.D. student	Ph.D. student
Department of Chemical and Biomolecular Engineering University of Delaware	Department of Materials Science and Engineering University of Delaware	Department of Materials Science and Engineering University of Delaware

Table of Contents

Abstract 3
Introduction 4
Project Goal 4
Computational Approach 5
Topology Generation 5
Non-Equilibrium Molecular Dynamics Simulation and Density of States Analysis 6
Simulated Systems 7
Results 7
Conclusions 8
Acknowledgements and CrediT 9
Appendix 9
A. Bonded and Nonbonded Potentials in the OPLS-AA Force Field 9
B. Radial Distribution Function Plots for Each Diol 9
C. Mass Density Profiles 10
D. Spatial Temperature Profiles and Number of Atoms in NEMD Simulation 11
E. Results and Error Estimation for Linear Regression for System Size Correction 12
F. Simulation Speed and Efficiency 13
G. Proposed Modifications to the OPLS-AA Force Field 14
References 14

Abstract

Polyurethane (PU) foams are widely used as thermal insulation materials due to their low thermal conductivity. While gas-phase conduction has been well studied, a significant portion of heat is transferred through the solid polymer matrix, which is known as solid conduction. However, experimental investigation of solid conduction is challenging, and molecular dynamics (MD) simulations can study thermal conductivity in a time and cost-efficient way. In this project, we developed an automated topology generation workflow to efficiently construct system topologies of polyurethane (PU) polyol monomers with the OPLS-AA force field for simulation with the LAMMPS software package. We constructed the topology generation workflow using open-source tools, including the Python packages mBuild and Foyer, to facilitate intellectual property protection. Using this topology generation workflow with atomistic non-equilibrium molecular dynamics (NEMD) simulations, we computed density, thermal conductivity, and constant-volume heat capacities of liquid 1,6-hexanediol (H-diol), 2,2,3,3,4,4,5,5-octafluoro-1,6-hexanediol (F-diol), and diethylene glycol (E-diol), and evaluated structure-property relationships that may inform the design of future thermal insulation materials.

Introduction

In the U.S., buildings contribute around 29% of total greenhouse gas emissions, largely from energy used for heating, cooling, and water heating which alone makes up 18% of a typical home's energy use.[1] The EPA estimates that adding insulation and air sealing can cut heating and cooling costs by 15%. Nearly 89% of homes are under-insulated, and so improving insulation offers a major opportunity for reducing energy use and emissions.[2]

Polyurethane (PU) foams are widely used for insulation due to their low thermal conductivity, which results from their closed-cell structure and the polymer's inherent thermal properties. PU is formed by reacting polyols, molecules containing multiple hydroxyl (alcohol) groups, with diisocyanates, often with a blowing agent to create the foam. The structure of PU can include hard and soft segments and functional groups like ethers, esters, aromatics, and ureas, enabling a wide range of mechanical and thermal properties.[1]

The thermal transport in PU foams involves gas-phase conduction through trapped gases, solid-phase conduction through the polymer matrix, and radiative transfer across pores. While gas-phase conduction is well studied, via experimental measurements[2] and coarse-grained MD simulations[3,4], solid-phase conduction has seen little investigation.[5,6] Accurately measuring the thermal properties of solid PU is challenging due to the difficulty of synthesizing void-free samples. The high viscosity of the reacting components can trap ambient gases during mixing, and additional CO_2 can be generated from side reactions between isocyanates and trace moisture.

To address these challenges, we employed atomistic MD simulations as a powerful tool for investigating heat conduction at the molecular scale. MD simulation allows us to elucidate how factors such as chain alignment, diol chemistry, and molecular-level ordering influence thermal transport. However, manually preparing topologies to simulate a variety of PU chemistries, by specifying the molecular structure and bonded and nonbonded interactions of each new chemistry, would be time-consuming and possibly error prone. Therefore, we developed a workflow using open-source tools to automatically construct all-atom initial configurations of polyol monomers, parameterized with the OPLS-AA force field for simulations. This approach enables a bottom-up investigation of structure–property relationships of polyols, with the long-term goal of guiding the design of more thermally efficient polymeric insulation materials. In future work, this workflow may be extended to diisocyanate monomers and PU polymers.

Project Goal

Investigate solid-phase heat conduction in PU systems using atomistic MD simulations. This study has the following objectives:

Objective 1: Build chemically consistent 3D molecular structures of polyol monomers.

Objective 2: Apply the OPLS-AA force field to specify bonded and non-bonded interactions.

Objective 3: Generate system topologies for assemblies of polyol monomers.

Objective 4: Perform atomistic non-equilibrium MD (NEMD) simulations with the generated topologies to compute the mass densities and thermal properties of polyol monomers, and to analyze how their molecular structure influences thermal transport.

Hypothesis: Thermal properties from simulation will reflect experimentally observed trends for liquid polyols, such as higher thermal resistance for fluorinated vs non-fluorinated polyols[7,8] and for polyols with weaker intermolecular interactions.

Computational Approach

Various computational methods are used to study thermal transport in soft materials across different scales.[3,9-11] In this study, we employ molecular dynamics (MD) simulations because they are less computationally intensive than quantum-scale methods and can capture larger-scale structural features like chain alignment, which influence thermal transport pathways. Post-simulation corrections can also be applied to account for quantum effects not captured during in classical atomistic simulation.[10]

The choice of molecular model affects both the accuracy and cost of simulation. We used an all-atom model to capture subtle differences in PU chemistry without needing custom coarse-graining.[12,13] Additionally, the explicit representation of hydrogen atoms affects both intra- and intermolecular interactions across all PU chemistries, which we expect to be particularly relevant when comparing the simulation behavior of fluorinated and non-fluorinated chemistries. We selected the all-atom version of the **O**ptimized **P**otentials for **L**iquid **S**imulations – **A**ll **A**tom (OPLS-AA) force field[14] on account of its accessibility and wide application in literature, including in the study of PU systems.[15,16]

To conduct a simulation, the positions and bonds for all atoms must be defined as well as the functional forms and parameters for all bonded and nonbonded interactions, which is collectively known as the system's topology. Manually creating the topology for each chemistry for each system would be time-consuming and possibly error-prone, so we developed a workflow (**Error! Reference source not found.**) to create an initial configuration of polyol monomers and apply the OPLS-AA force field. We then performed MD simulations and analyzed the simulation data to assess the mass density, thermal conductivity, and constant-volume heat capacity of select polyols in the liquid phase.

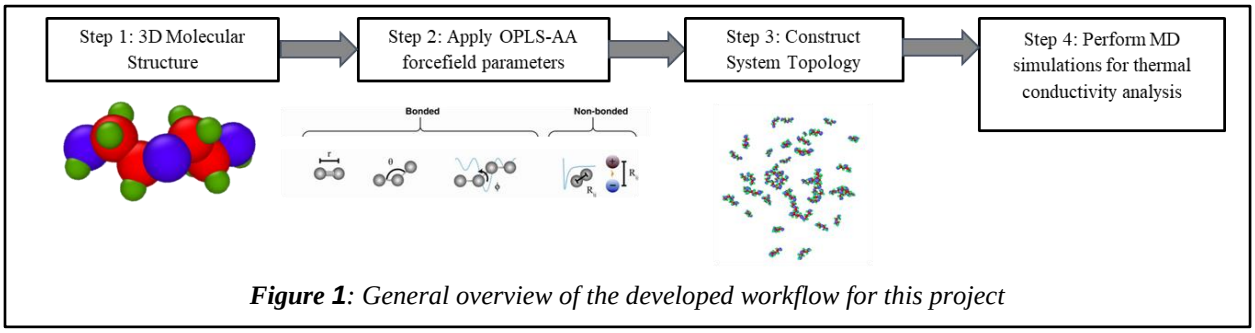

***Figure 1**: General overview of the developed workflow for this project*

Topology Generation

In molecular dynamics simulations, topology refers to structural and interaction information that defines a molecular system for simulation. It describes how atoms are connected via well-defined bonded and non-bonded interactions (e.g., bond stretching, angle bending, van der Waals forces), how they interact, and what force field parameters govern their behavior. The functional forms of the potentials in the OPLS-AA force field are listed in Appendix section A.

We used open-source Python tools made by the **M**olecular **S**imulation **D**esign **F**ramework (MoSDeF)[17] project to simplify simulation setup and ensure reproducibility across different simulation engines. The mBuild[18] Python package was used to help build complex molecules and automatically kept track of how atoms are connected in space. The Foyer package[19] was utilized to apply OPLS-AA parameters. In a nutshell, Foyer helps apply and share force fields used in molecular modeling. To assign each atom a "type" with corresponding (non)bonded parameters, Foyer uses SMiles Arbitrary Target Specification (SMARTS) patterns, and "overrides" help decide which atom types take priority for a specific force field.

We used open-source Python tools made by **M**olecular **S**imulation **D**esign **F**ramework (MoSDeF)[17] project to simplify simulation setup and ensure reproducibility across different simulation engines.

We validate our workflow with three diols, 1,6-hexanediol (H-diols), 2,2,3,3,4,4,5,5-octafluoro-1,6-hexanediol (F-diols), and diethylene glycol (E-diols) (**Error! Reference source not found.**). mBuild converts the SMILES string of the diols into a 3D molecular structure, and then Foyer is used to apply OPLS-AA force field parameters by assigning a proper atom type to each atom. This initial configuration is generated at a low density, $0.02\ g/cm^3$, to facilitate molecule placement.

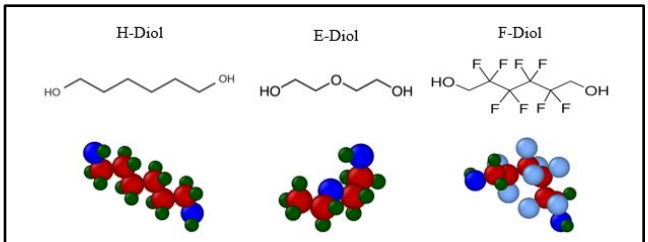

***Figure 2**: The 3 diols used in our topology generation step*

Non-Equilibrium Molecular Dynamics Simulation and Density of States Analysis

We performed MD simulations with the LAMMPS software package.[20] We used non-equilibrium molecular dynamics (NEMD) simulation for thermal property analysis; specifically, we used the Muller-Plathe formalism for reverse NEMD[21] which is pre-implemented in the base version of LAMMPS. We performed a density of states (DOS) analysis[10,22] on each system to correct for quantum-scale effects on thermal transport which are not represented in our classical MD simulations. All simulations were conducted with a timestep of $1\ fs$, unless otherwise specified, in a periodic simulation volume. The simulation temperature was maintained at $350\ K$ throughout each simulation to match experimental conditions and remain well above the melting temperatures of each diol.[6,23,24]

We first shrank the simulation volume to increase the system's mass density to $0.9\ g/cm^3$ to reasonably approximate the density of most liquid polyols.[23,24] The shrinkage was performed over $1\ ns$ (10^6 timesteps) at $350\ K$ with a Nose-Hoover thermostat[25,26] with a coupling constant of $100\ fs$. Following this, we equilibrated the system for $1\ ns$ at $350\ K$ and $1\ g/cm^3$ in the NVT ensemble; we then applied the Nose-Hoover barostat to transition to the NPT ensemble and equilibrated at $350\ K$ and $1\ atm$ for $30\ ns$. To sample the equilibrium mass density of each diol liquid, we simulated 1000 monomers of each diol using this protocol and sampled their density every $0.1\ ns$ for the final $10\ ns$ of equilibration.

We performed a DOS analysis for each system to correct the thermal properties derived from simulation.[10,22] All of the bonded interactions in a simulated molecule contribute vibrational modes that facilitate thermal transport, whereas in reality high frequency modes contribute little to thermal transport near ambient temperatures. We calculated a correction factor as outlined by Mukherji[10] by first finding the vibrational DOS spectra as the Fourier transform of atom velocity autocorrelation, normalized such that the area under the curve is 1. We then calculated the correction factor as the integral of the DOS profile weighted by the temperature derivative of the probability of activation[22,27,28] at $350\ K$. We also used the DOS analysis to find the constant-volume heat capacity in simulation as the product of the integral of the DOS spectra and the ideal gas heat capacity. To sample the velocity autocorrelation profile, we continued NVT simulation of the final configuration from the previous simulation step with a timestep of $0.5\ fs$ and sampled velocity autocorrelation at every timestep for $5\ ps$.

To assess the diol thermal conductivity, we proceeded (unless noted otherwise) with reverse NEMD simulation using the final configuration of the NPT relaxation step. We divided the simulation volume into 10 zones of equal volume along one axis and established a "hot" zone (z-axis origin) and "cold" zone (z-

axis middle, to account for periodic boundaries) by periodically swapping particle kinetic energies to create a heat flux. We performed the energy swap every 100 fs over 1 ns of simulation to develop a steady-state temperature gradient $\left({}^{dT}/_{dz}\right)$ and then sampled ${}^{dT}/_{dz}$ every 0.1 ns over an additional 1 ns. We calculated the thermal conductivity according to Fourier's law using this temperature profile and the heat flux, found as the exchanged kinetic energy divided by xy-plane cross-sectional area and the sampling interval (0.1 ns).

Simulated Systems

To account for finite-size effects on thermal transport in simulation[29], we sampled thermal properties from simulations of each diol of varying dimensions. We prepared simulations with z-axis lengths of 8, 10, 12, 20, and 24 nm to vary the distance over which the temperature gradient was applied. We specified the x and y axes lengths of 4.5 nm to avoid molecule self-interaction and picked the number of molecules in each system so that the mass density of the simulations of the chosen dimensions would approach the previously sampled equilibrium mass densities. We elaborate on the finite-size correction in the next section and in Appendix section E.

Results

We used our topology generation workflow to create simulations of liquid diols. The generation process takes from ~2 to 15 minutes (1 CPU core) depending on the number of molecules and target density, and significant optimization is likely possible.

Table 1 *Comparison of mass density (ρ) of diol monomer from simulation (this work) and experiment. All values are given as the average ± 1 standard deviation, where the variance is known.*

	$\rho_{sim}\ \left({}^{g}/_{cm^3}\right)$	$\rho_{exp}\ \left({}^{g}/_{cm^3}\right)$
E-Diol	1.01 ± 0.00	1.11[23]
H-Diol	0.9 ± 0.00	0.92 ± 0.01[24]
F-Diol	1.55 ± 0.01	1.50*

** Data provided by Tom Fielitz at Dow Chemical Company*

The mass densities sampled from the first set of simulations were compared with experimental values in Table 1. The equilibration of the simulated liquid diols is supported by the stability of the simulation mass density over time across the sampling period (Appendix C.1). The simulation densities agreed well with those from experiments, with the greatest divergence observed for E-diol. This correspondence is highly relevant to the thermal property analysis as thermal transport is influenced by the proximity and ordering of molecules, particularly for these systems of individual monomers. Therefore, a discrepancy in equilibrium density could significantly increase the error in thermal properties from simulation.

Table 2 *Comparison of thermal conductivity (k) and constant-volume heat capacities (C_V) of diol monomers from simulation (this work) and experiment. Simulation results have had the DOS correction incorporated. All values are given as the average ± 1 std. dev., where the variance is known.*

	$k_{sim}\ \left({}^{W}/_{mK}\right)$	$k_{exp}\ \left({}^{W}/_{mK}\right)$	$C_{V,sim}\ \left({}^{J}/_{mol*K}\right)$	$C_{V,exp}\ \left({}^{J}/_{mol*K}\right)$
E-Diol	0.165 ± 0.014	0.201 ± 2%[30]	294 ± 4	309 ± 1[31]
H-Diol	0.165 ± 0.013	0.200 ± 1%[32]	314 ± 5	327 ± 6[24]
F-Diol	0.090 ± 0.006	0.090*	152 ± 2	366 ± 1*

** Data provided by Tom Fielitz at Dow Chemical Company*

We calculated the thermal conductivity and constant-volume heat capacity of each diol (Table 2) from the velocity autocorrelation functions and z-axis temperature profiles sampled from each simulation. See Appendix section D for example temperature profiles. We first found the classical (non-corrected) thermal conductivity at infinite system size by extrapolating from the simulations results of varying z-axis length (see Appendix section E for details) and the classical heat capacity and then applied the DOS correction, averaged over all simulations of each diol. We did not observe significant finite-size effects on the heat capacity, so the heat capacity values in Table 2 are the average across systems of all sizes for each diol. The thermal conductivities from NEMD simulation are in good agreement with experimental values; in particular, the simulation and experimental values were within error of each other (although the error for the experimental thermal conductivity and heat capacity for F-diol was not known to us). Both values for the E and H diols were not equal within uncertainty; their simulated and experimental heat capacities were also similar but distinct within uncertainty. However, significant deviation was observed for the F diol heat capacity despite the correspondence for its thermal conductivity values. The difference in agreement for F-diol thermal conductivity and heat capacity may be attributable to how the OPLS-AA forcefield parameterizes fluorine atoms.[33] We elaborate on the possible causes and solutions for the discrepancy in F-diol thermal properties in Appendix section G.

Conclusions

In this work, we created a topology generation workflow for the diol components of polyurethane for thermal property analysis with NEMD simulation. The generation workflow is constructed entirely with open-source Python packages, making it free to use on offline systems for protection of intellectual property. We used the topology generation workflow to initialize simulations of the E, H, and F diols to sample mass density, thermal conductivity, and constant-volume heat capacities. Overall, we found good agreement between our predicted properties and experimental values, with $\leq$ 25% deviation for all properties except the F-Diol heat capacity. The data partially support our hypothesis: the thermal conductivity of fluorinated polyols is significantly reduced vs non-fluorinated polyols in simulation, in agreement with experiment. However, the heat capacities from simulation do not reflect the weak dependence of heat capacity on fluorination as observed in experiment.

Possible extensions to this work include updating the OPLS-AA parameters for fluorine for more accurate thermal properties and incorporating parameters for urethane groups and other moieties found in PU into Foyer to extend the topology generation framework to PU polymer chains. These parameters may be sourced from literature[16] or derived from experimental data (see Appendix section G) or high-level quantum calculations. The reverse NEMD method we used may be replaced with other (non)equilibrium simulation methods, such as approach to equilibrium (ATE) or Green-Kubo analysis; the latter enables the analysis of directional heat transport, which may be of interest in PU materials.

Acknowledgements and CrediT

This work was carried out by team members Siyuan Liu (presentation lead), Tristan Myers (technical lead), and Tamem Salah (communications and team lead). Siyuan Liu contributed to conceptualization, methodology, resources, and visualization. Tristan Myers contributed to conceptualization, methodology, resources, software, and visualization. Tamem Salah contributed to conceptualization, methodology, resources, software, and visualization. The team gratefully acknowledges the guidance of industry mentors Dr. Tom Fielitz and Dr. Puja Agarwala from Dow Chemical Company. Additional support was provided by course instructor Professor Arthi Jayaraman and teaching assistant Jay Shah at the University of Delaware. Computational resources were provided by the DARWIN High-Performance Computing (HPC) cluster at the University of Delaware.

Appendix

A. Bonded and Nonbonded Potentials in the OPLS-AA Force Field

The functional forms of the potentials in the OPLS-AA force field are:

$$E_{bond} = \sum_{bonds} K_r(r - r_0)^2$$

$$E_{angles} = \sum_{angles} K_\theta(\theta - \theta_0)^2$$

$$E_{dihedrals} = \sum_{dihedrals} (\frac{V_1}{2}[1 + \cos(\phi - \phi_1)] + \frac{V_2}{2}[1 + \cos(2\phi - \phi_2)] + \frac{V_3}{2}[1 + \cos(3\phi - \phi_3)] + \frac{V_4}{2}[1 + \cos(4\phi - \phi_4)])$$

$$E_{nonbonded} = \sum_{i>j} f_{ij}(\frac{A_{ij}}{r_{ij}^{12}} - \frac{C_{ij}}{r_{ij}^{6}} + \frac{q_i q_j e^2}{4\pi\epsilon_0 r_{ij}})$$

With a standard combining rule for LJ interactions $A_{ij} = \sqrt{A_{ii}A_{jj}}$ and $C_{ij} = \sqrt{C_{ii}C_{jj}}$.

B. Radial Distribution Function Plots for Each Diol

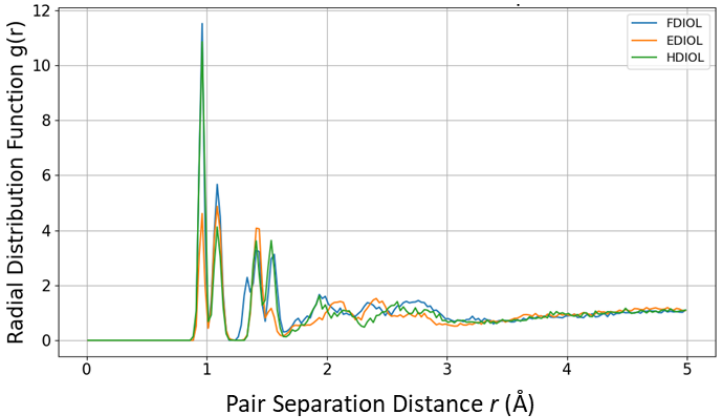

Figure B.1 *Radial distribution function plots between every pair of atoms for all 3 diols. Atom positions were sampled in the same way as mass density - every 0.1 ns over the final 10 ns of NPT relaxation (350 K, 1 atm).*

These radial distribution function (RDF) profiles indicate that E-diol has more diffuse RDF peaks indicating lower structural rigidity and less localized clustering due to weaker hydrogen-bonding networks. H-diol forms compact, hydrogen-bonded aggregates due to interactions between aliphatic hydrogens along

the backbone and terminal hydroxyl groups. Lastly, in F-diol, the fluorinated backbone increases backbone conformational rigidity and dipole-dipole interaction due to the high polarity of fluorine, promoting tighter packing and strong intermolecular interactions around $r = 1 - 2$ Å. Additionally, the general OPLS-AA force field has been shown to overestimate the stiffness and conformational rigidity of fluorinated polymers. Studies on Polytetrafluoroethylene reported that OPLS-AA predicted a characteristic ratio of 28 (vs. experimental 8 ± 2.5), with missing conformational states and dynamics an order of magnitude too slow.[33] These issues may also manifest in F-diol systems, leading to artificially enhanced local packing, sharp RDF peaks, and distorted vibrational spectra, ultimately contributing to disagreements in predicted heat capacity (as shown in table 2).

C. Mass Density Profiles

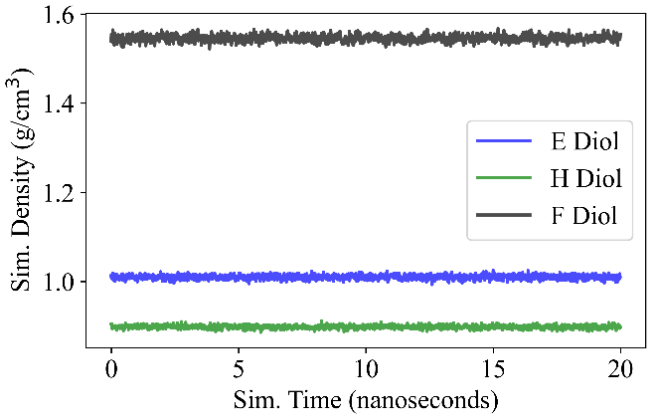

Figure C.1 *Profiles of mass density for liquid diols of 1000 molecules of each diol, sampled at each timestep (1 fs) from the last 20 ns of simulation in the NPT ensemble at 350 K and 1 atm.*

D. Spatial Temperature Profiles and Number of Atoms in NEMD Simulation

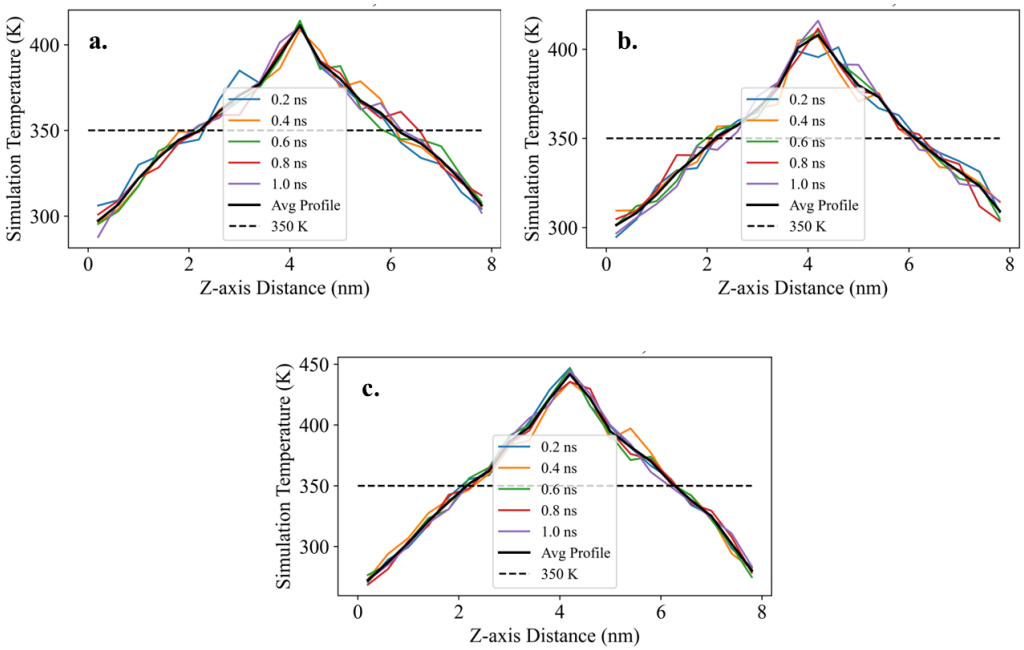

Figure D.1 *Sample z-axis temperature profiles for simulations of liquid (a) E-diol, (b) H-diol, and (c) F-diol with an* 8 *nm z-axis length. Each profile is sampled from a single timestep, and the timepoint given for each profile is the simulation time during the* 1 *ns sampling period at which the profile was sampled. An averaged temperature profile is marked with a bold line, and the target system temperature of* 350 *K is marked with a dashed line.*

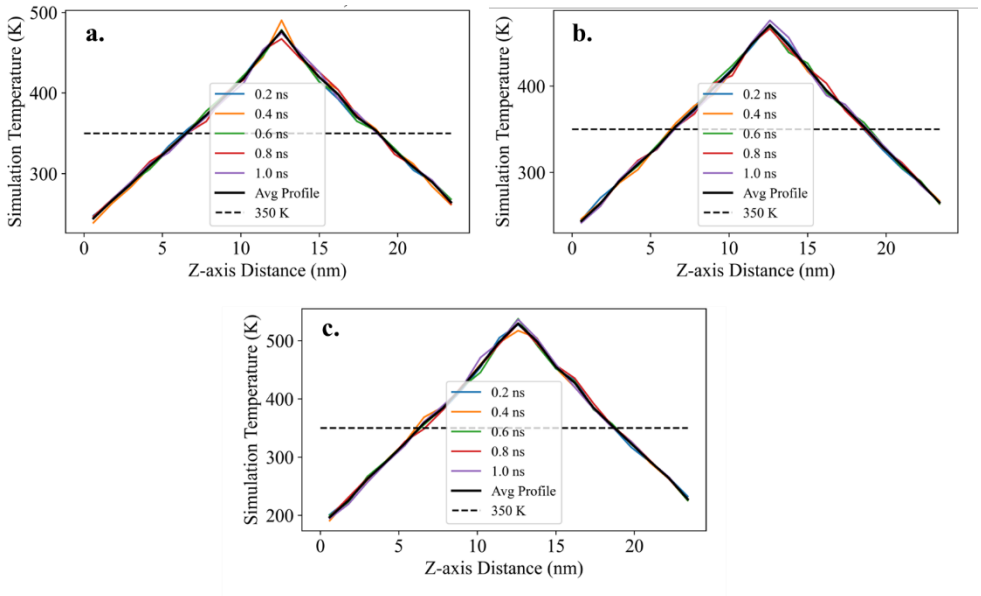

Figure D.2 *Sample z-axis temperature profiles for simulations of liquid (a) E-diol, (b) H-diol, and (c) F-diol with an* 24 *nm z-axis length. The layout of each figure and sampling of temperature profiles are the same as with Figure D.1.*

Table D.1 *Number of atoms in diol simulations of varying z-axis length. The E, H, and F diols have 17, 22, and 22 atoms respectively.*

	8 nm	**10 nm**	**12 nm**	**20 nm**	**24 nm**
E Diol	15640	19550	23460	39100	47090
H Diol	16280	20240	24200	40480	48620
F Diol	12980	16280	19580	32560	38940

E. Results and Error Estimation for Linear Regression for System Size Correction

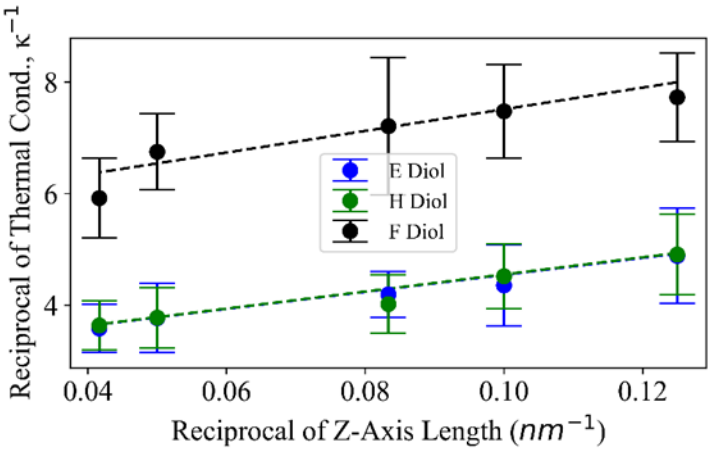

Figure E.1 *Reciprocal of average thermal conductivity vs reciprocal of system z-axis length and linear fits (dashed line) of E, H, and F diols. Error bars are 1 standard deviation.*

Thermal transport in simulation has a significant dependence on system size, which can be accounted for by calculating thermal properties from simulations of different sizes (different z-axis lengths, in our case) and extrapolating to the properties of system of infinite size. The dependence of thermal conductivity on the distance of thermal transport is such that the reciprocals of these two quantities should be proportional. Accordingly, the thermal conductivity at infinite system size k_{inf} is found with the y-intercept y_0 of the linear fit of reciprocal thermal conductivity vs reciprocal z-axis length (where the z-axis is the direction of thermal transport in NEMD simulation). The thermal conductivity k_{inf} is the reciprocal of the intercept, so $k_{inf} = y_0^{-1}$. The error in k_{inf} is estimated with the following expression:

$$\sigma_{k\_inf} = \frac{d}{d(y_0)}(y_0^{-1})\sigma_{y0} = \frac{\sigma_{y0}}{y_0^2}$$

In the above, σ_{y0} is the standard error in y_0.

Table E.1 k_{inf} $\left({}^{W}/_{mK}\right)$ *from regression after sequential removal of k from the shortest (rightmost along horizontal axis) and the longest (leftmost) systems*

Removed Datapoints	**E Diol**	**H Diol**	**F Diol**

3 leftmost	0.711	0.201	0.106
2 leftmost	0.268	0.348	0.204
1 leftmost	0.304	0.326	0.198
None	0.296	0.312	0.181
1 rightmost	0.276	0.329	0.193
2 rightmost	0.341	0.250	0.134
3 rightmost	0.201	0.279	0.123

To get another estimation of the error in k_{inf}, we sequentially removed the thermal conductivity of the shortest or longest box size from the regression and re-calculated k_{inf} with the truncated data. We present the regressed k_{inf} from removal of the shortest (rightmost along horizontal axis) and longest (leftmost) systems in Table E.1.

F. Simulation Speed and Efficiency

Table F.1 Simulation speed (light blue) in ns/day for each simulation stage for E-diol liquid simulations, calculated as the quotient of the simulation duration in ns (simulation time) and days (wall time). All simulations were performed on the DARWIN supercomputing cluster (U Delaware) on 32-core AMD EPYC 7002 series processors (note that not all cores on a given processor were allocated to each simulation stage). These data are plotted against the number of atoms in **Fig. F.3**.

Simulation Scale						
Z-axis Length (nm)			8	10	12	20	24
Number of Atoms			15640	19550	23460	39100	47090
Simulation Protocol	**Simulation Stage Length (ns)**	**CPU Cores**					
NPT Relaxation	30	30	12.7	8.7	8.7	5.0	3.1
Sampling of Velocity Autocorr.	0.005	8	2.1	1.6	1.4	0.9	0.7
NEMD Simulation	2	8	3.7	2.9	2.5	1.4	1.2

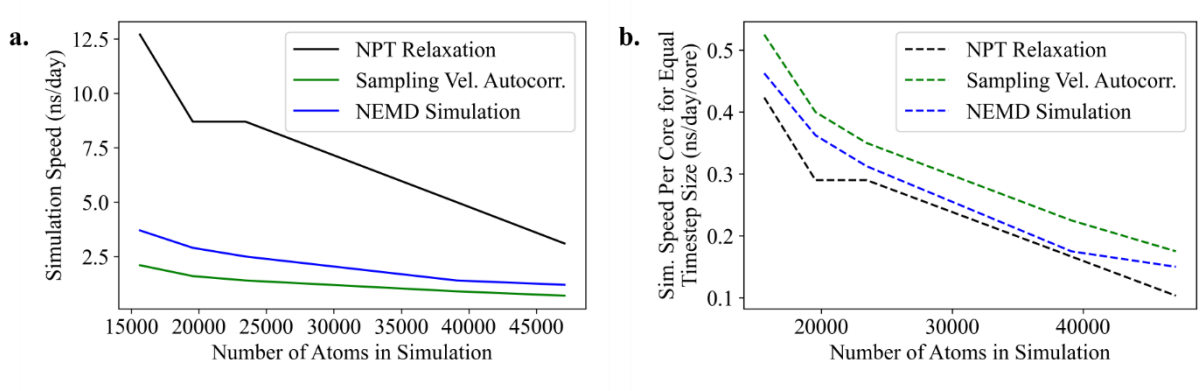

Figure F.3 *(a) Simulation speed data in* ***Table F.1*** *plotted against the number of atoms in simulation. (b) Simulation speed per core with a consistent timestep of 1 fs against the number of atoms in simulation. For (b), we assume the simulation speed would double if the timestep in the "Sampling Velocity Autocorrelation" stage ~~were~~was doubled from 0.5 to 1 fs.*

G. Proposed Modifications to the OPLS-AA Force Field

The difference in agreement for F-diol thermal conductivity and heat capacity suggests that the intermolecular thermal transport (thermal conductivity) of F-diol is well represented within our simulations, but that the storage of thermal energy is not. Nonbonded interactions facilitate thermal transport between the diol molecules, and the agreement in thermal conductivity values suggests that the OPLS-AA nonbonded parameters as implemented are accurate. The discrepancy in heat capacity suggests that the bonded interactions that govern intramolecular energy storage should be revised.

To improve agreement between simulation results and experimental conductivity values, we propose to fit the density of states (DOS) spectra with experimental vibrational data by adjusting the OPLS-AA bonded parameters. While the DOS spectra computed from simulation captures all vibrational modes, whether or not the modes are active in the infrared range, experimental Fourier Transform Infrared Spectroscopy (FTIR) spectra only reflects dipole-active transitions. Nevertheless, both spectra should share common peak positions corresponding to fundamental molecular motions (e.g., bond stretching, bending, torsion). We propose compare the DOS plots obtained from MD simulation results with FTIR spectra and align the low-to-mid frequency peaks. This allows meaningful comparison of peak frequencies, which represent the vibrational modes governing phonon transport. While the most attention should be paid to the bonded parameters in order to rectify the simulated heat capacity of F-diol, it may be necessary to simultaneously adjust the nonbonded interactions (described with the Coulombic and Lennard-Jones potentials) to preserve accuracy for all material properties.

References

1 Ates, M., Karadag, S., Eker, A. A. & Eker, B. Polyurethane foam materials and their industrial applications. *Polymer International* **71**, 1157-1163 (2022). https://doi.org/https://doi.org/10.1002/pi.6441

2 Reichenauer, G., Heinemann, U. & Ebert, H. P. Relationship between pore size and the gas pressure dependence of the gaseous thermal conductivity. *Colloids and Surfaces A: Physicochemical and Engineering Aspects* **300**, 204-210 (2007). https://doi.org/https://doi.org/10.1016/j.colsurfa.2007.01.020

3 Park, S., Moon, J., Kim, B. & Cho, M. Multi-scale coarse-grained molecular dynamics simulation to investigate the thermo-mechanical behavior of shape-memory polyurethane copolymers. *Polymer* **213**, 123228 (2021). https://doi.org/https://doi.org/10.1016/j.polymer.2020.123228
4 Uddin, M. S. & Ju, J. Enhanced Coarse-Graining of Thermoplastic Polyurethane Elastomer for Multiscale Modeling. *Journal of Engineering Materials and Technology* **139** (2016). https://doi.org/10.1115/1.4034328
5 Zhou, J. *et al.* Reduction of the Thermal Conductivity of Polyurethanes by Fluorination: Impact of Crystallinity, Atomic Density, and Sound Velocity. *Angewandte Chemie* (2025). https://doi.org/10.1002/ange.202503497
6 Zhou, J. *et al.* Thermal Conductivity of Polyurethane Thin Films. *Macromolecules* **57**, 6838-6847 (2024). https://doi.org/10.1021/acs.macromol.4c00401
7 Yata, J., Minamiyama, T. & Tanaka, S. Measurement of thermal conductivity of liquid fluorocarbons. *International Journal of Thermophysics* **5**, 209-218 (1984). https://doi.org/10.1007/bf00505501
8 Sun, J. *et al.* Probe beam deflection technique with liquid immersion for fast mapping of thermal conductance. *Applied Physics Letters* **124** (2024). https://doi.org/10.1063/5.0179581
9 Sachar, H. S., Chava, B. S., Pial, T. H. & Das, S. All-Atom Molecular Dynamics Simulations of the Temperature Response of Densely Grafted Polyelectrolyte Brushes. *Macromolecules* **54**, 6342-6354 (2021). https://doi.org/10.1021/acs.macromol.1c00922
10 Mukherji, D. Computing the thermal transport coefficient of neutral amorphous polymers using exact vibrational density of states: Comparison with experiments. *Physical Review Materials* **8** (2024). https://doi.org/10.1103/PhysRevMaterials.8.085601
11 Gartner, T. E. & Jayaraman, A. Modeling and Simulations of Polymers: A Roadmap. *Macromolecules* **52**, 755-786 (2019). https://doi.org/10.1021/acs.macromol.8b01836
12 Wang, H., Junghans, C. & Kremer, K. Comparative atomistic and coarse-grained study of water: what do we lose by coarse-graining? *Eur Phys J E Soft Matter* **28**, 221-229 (2009). https://doi.org/10.1140/epje/i2008-10413-5
13 Schiller, U. D., Kruger, T. & Henrich, O. Mesoscopic modelling and simulation of soft matter. *Soft Matter* **14**, 9-26 (2017). https://doi.org/10.1039/c7sm01711a
14 Jorgensen, W. L., Ghahremanpour, M. M., Saar, A. & Tirado-Rives, J. OPLS/2020 Force Field for Unsaturated Hydrocarbons, Alcohols, and Ethers. *J Phys Chem B* **128**, 250-262 (2024). https://doi.org/10.1021/acs.jpcb.3c06602
15 Vakili, H. *et al.* Self-assembly of a patterned hydrophobic-hydrophilic surface by soft segment microphase separation in a segmented polyurethane: Combined experimental study and molecular dynamics simulation. *Polymer* **195** (2020). https://doi.org/10.1016/j.polymer.2020.122424
16 Ghermezcheshme, H., Makki, H., Mohseni, M., Ebrahimi, M. & de With, G. MARTINI-based simulation method for step-growth polymerization and its analysis by size exclusion characterization: a case study of cross-linked polyurethane. *Phys Chem Chem Phys* **21**, 21603-21614 (2019). https://doi.org/10.1039/c9cp03407b
17 Cummings, P. T. *et al.* Open‐source molecular modeling software in chemical engineering focusing on the Molecular Simulation Design Framework. *AIChE Journal* **67** (2021). https://doi.org/10.1002/aic.17206
18 Klein, C. *et al.* in *Foundations of Molecular Modeling and Simulation Molecular Modeling and Simulation* Ch. Chapter 5, 79-92 (2016).
19 Klein, C. *et al.* Formalizing atom-typing and the dissemination of force fields with foyer. *Computational Materials Science* **167**, 215-227 (2019). https://doi.org/10.1016/j.commatsci.2019.05.026

20 Thompson, A. P. *et al.* LAMMPS - a flexible simulation tool for particle-based materials modeling at the atomic, meso, and continuum scales. *Computer Physics Communications* **271** (2022). https://doi.org/10.1016/j.cpc.2021.108171
21 Müller-Plathe, F. A simple nonequilibrium molecular dynamics method for calculating the thermal conductivity. *The Journal of Chemical Physics* **106**, 6082-6085 (1997). https://doi.org/10.1063/1.473271
22 Horbach, J., Kob, W. & Binder, K. Specific Heat of Amorphous Silica within the Harmonic Approximation. *The Journal of Physical Chemistry B* **103**, 4104-4108 (1999). https://doi.org/10.1021/jp983898b
23 Guard, U. C. Chemical hazard response information system (CHRIS)-hazardous chemical data. *Commandant Instruction* **16465** (1999).
24 Frenkel, M., Hong, X., Wilhoit, R. C. & Hall, K. R. in *Densities of Alcohols Landolt-Börnstein - Group IV Physical Chemistry* Ch. Chapter 4, 303-361 (2000).
25 Nose, S. A molecular dynamics method for simulations in the canonical ensemble. *Molecular Physics* **52**, 255-268 (1984).
26 Hoover, W. G. Canonical dynamics: Equilibrium phase-space distributions. *Phys Rev A Gen Phys* **31**, 1695-1697 (1985). https://doi.org/10.1103/physreva.31.1695
27 Wischnewski, A., Buchenau, U., Dianoux, A. J., Kamitakahara, W. A. & Zarestky, J. L. Neutron scattering analysis of low-frequency modes in silica. *Philosophical Magazine B* **77**, 579-589 (2009). https://doi.org/10.1080/13642819808204986
28 Taraskin, S. N. & Elliott, S. R. Nature of vibrational excitations in vitreous silica. *Physical Review B* **56**, 8605-8622 (1997). https://doi.org/10.1103/PhysRevB.56.8605
29 Schelling, P. K., Phillpot, S. R. & Keblinski, P. Comparison of atomic-level simulation methods for computing thermal conductivity. *Physical Review B* **65** (2002). https://doi.org/10.1103/PhysRevB.65.144306
30 DiGuilio, R. & Teja, A. S. Thermal conductivity of poly(ethylene glycols) and their binary mixtures. *Journal of Chemical & Engineering Data* **35**, 117-121 (2002). https://doi.org/10.1021/je00060a005
31 Stephens, M. A. & Tamplin, W. S. Saturated liquid specific heats of ethylene glycol homologs. *Journal of Chemical & Engineering Data* **24**, 81-82 (2002). https://doi.org/10.1021/je60081a027
32 Velliadou, D. *et al.* Accurate Measurements of the Thermal Conductivity of n-Docosane, n-Tetracosane, 1,6-Hexanediol, and 1,8-Octanediol in the Solid and Liquid Phases. *International Journal of Thermophysics* **44** (2023). https://doi.org/10.1007/s10765-023-03182-6
33 Borodin, O., Smith, G. D. & Bedrov, D. A Quantum Chemistry Based Force Field for Perfluoroalkanes and Poly(tetrafluoroethylene). *The Journal of Physical Chemistry B* **106**, 9912-9922 (2002). https://doi.org/10.1021/jp026158i